

FreeQ-Graph: Free-form Querying with Semantic Consistent Scene Graph for 3D Scene Understanding

Chenlu Zhan, Gaoang Wang *Member, IEEE*, Hongwei Wang *Member, IEEE*

Abstract—Semantic querying in complex 3D scenes through free-form language presents a significant challenge. Existing 3D scene understanding methods use large-scale training data and CLIP to align text queries with 3D semantic features. However, their reliance on predefined vocabulary priors from training data hinders free-form semantic querying. Besides, recent advanced methods rely on LLMs for scene understanding but lack comprehensive 3D scene-level information and often overlook the potential inconsistencies in LLM-generated outputs. In our paper, we propose FreeQ-Graph, which enables Free-form Querying with a semantic consistent scene Graph for 3D scene understanding. The core idea is to encode free-form queries from a complete and accurate 3D scene graph without predefined vocabularies, and to align them with 3D consistent semantic labels, which accomplished through three key steps. We initiate by constructing a complete and accurate 3D scene graph that maps free-form objects and their relations through LLM and LVLM guidance, entirely free from training data or predefined priors. Most importantly, we align graph nodes with accurate semantic labels by leveraging 3D semantic aligned features from merged superpoints, enhancing 3D semantic consistency. To enable free-form semantic querying, we then design an LLM-based reasoning algorithm that combines scene-level and object-level information to intricate reasoning. We conducted extensive experiments on 3D semantic grounding, segmentation, and complex querying tasks, while also validating the accuracy of graph generation. Experiments on 6 datasets show that our model excels in both complex free-form semantic queries and intricate relational reasoning.

Index Terms—3D Scene Understanding, Multi-modal Large Language Models, Scene Graph, Semantic Segmentation

I. INTRODUCTION

Interacting with 3D scenes using open-vocabulary perception is a key challenge facing current AI-driven agents [1], [2]. Accurately querying semantic objects and their relationships through complex free-form queries in intricate 3D environments remains an unresolved issue [3].

Recent works [4]–[6] tackling 3D scene understanding tasks frequently rely on CLIP [7] to align textual queries with scene semantics, which heavily depends on large-scale pre-trained datasets. Meanwhile, some methods leverage large language models (LLMs) [6], [8], [9] to facilitate flexible semantic interactions, which are crucial for handling complex queries in 3D scene understanding. We aim to develop a

This work was supported in part by Zhejiang Provincial Natural Science Foundation of China (LDT23F02023F02) and the National Natural Science Foundation of China (No.62106219). *Corresponding Authors: Hongwei Wang and Gaoang Wang.*

Chenlu Zhan is with the College of Computer Science and Technology, Zhejiang University, Zhejiang, China (chenlu.22@intl.zju.edu.cn)

Gaoang Wang, and Hongwei Wang are with Zhejiang University-University of Illinois Urbana-Champaign Institute, Zhejiang University, Haining, China. (gaoangwang@intl.zju.edu.cn, hongweiwang@intl.zju.edu.cn)

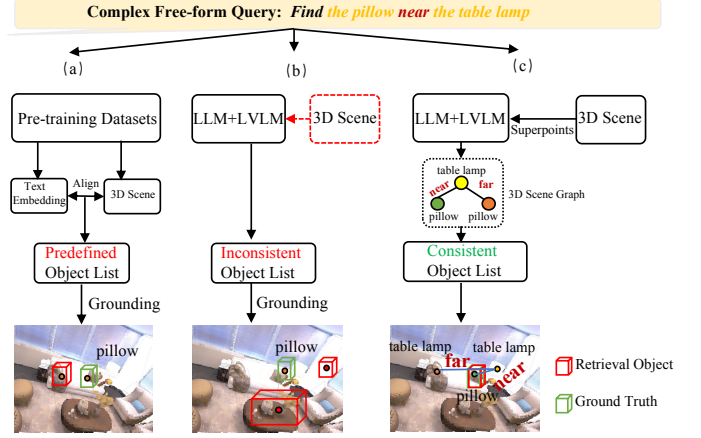


Fig. 1. We introduce FreeQ-Graph, a 3D scene understanding work for free-form complex semantic querying with a semantic consistent scene graph. (a) The open-vocabulary methods depend on pre-trained data and predefined objects to align text with 3D features, limiting their support for free-form queries. (b) Some methods overly depend on LLMs and LVLMs for reasoning, yet their lack of 3D scene awareness often yields object lists misaligned with actual 3D semantics, leading to inaccurate reasoning. (c) We propose a training-free framework that leverages LVLMs and LLMs to build a complete 3D spatial scene graph for free-form querying without predefined priors. Superpoint merging ensures the alignment of 3D node features with correct semantic labels, enabling accurate and consistent 3D scene understanding.

training-free framework that can acquire semantically aligned 3D features to support accurate free-form querying in 3D scenes. However, existing methods still encounter significant limitations: **1) Limited predefined vocabulary priors from training datasets hinder free-form semantic querying.** Most 3D scene understanding models [10]–[12] depend on large-scale training data and use CLIP to encode queries and scenes, inherently constraining them to a fixed set of predefined categories. This limitation hinders their capacity for free-form semantic querying and relational reasoning, as illustrated in Fig. 1 (a). **2) Inconsistency between 3D instance features and semantic labels.** Recent methods [6], [9], [13], [14] rely solely on LLMs and LVLMs to generate semantic labels for 3D instance features, yet neglect the lack of 3D scene information. This often leads to inconsistent or incorrect outputs, where objects and relations misalign with true 3D semantics, resulting in unreliable reasoning, as shown in Fig. 1(b). **3) Lack of scene spatial relation reasoning.** Current methods [15], [16] predominantly focus on object-level segmentation and retrieval, while disregarding spatial relationships within complex scenes. This oversight substantially constrains their capability to handle semantic relationship queries.

In our paper, we propose FreeQ-Graph, a training-free framework that enables free-form semantic querying with a

semantic consistent scene graph for 3D scene understanding. Our key innovation lies in a training-free, free-form querying framework that constructs a scene graph with accurate nodes and relations, aligns 3D instances with correct semantics through superpoint merging, and integrates LLM-based reasoning for spatial queries, setting our approach apart. 1) We construct a complete and accurate 3D scene graph using LVLMs and LLMs to map free-form instances and their relationships, without relying on any training priors. Unlike ConceptGraph [13], which depends on 2D models and often misses or duplicates objects, our approach ensures accurate scene representation through mutual correction between agents and the grounded model. 2) We align free-form nodes with consistent semantic labels to obtain 3D semantically consistent representations. This is achieved by generating superpoints and performing structural clustering to extract 3D instance features and their semantic labels, thereby aligning each 3D point with its corresponding semantics. In contrast, others [13] struggle with a consistent semantic representation. 3) We develop an LLM-based reasoning algorithm that breaks complex queries into CoT-reasoning by combining scene and object-level information for free-form querying. In contrast, other [13] single strategy lacks scene context, limiting its query capabilities. We conduct thorough experiments on six datasets, covering 3D semantic grounding, segmentation, and complex querying tasks, while also validating the accuracy of scene graph generation. The results demonstrate that our model excels in handling complex semantic queries and relational reasoning. Our contributions are summarized as follows:

- We propose FreeQ-Graph, a training-free free-form querying framework with the semantic consistent scene graph and LLM-based reasoning algorithm for 3D scene understanding.
- We propose a 3D semantic alignment method that aligns 3D graph nodes with consistent semantic labels, enabling the extraction of free-form 3D semantic-aligned features.
- We introduce an LLM-based CoT-reasoning algorithm that combines scene-level and object-level information for scene spatial reasoning.
- Extensive experiments on 6 datasets demonstrate that our method excels in querying complex free-form semantics and relation reasoning perceptions.

II. RELATED WORK

1) *Open-Vocabulary 3D Scene Understanding*: Natural language querying in complex 3D scenes demands deep understanding of free-form semantics and relationships. Many prior works [10], [11], [17]–[21] rely on joint training with large-scale pretrained data to align 3D scenes and query embeddings, but their dependence on predefined vocabularies limits true free-form querying. Recent advanced methods [6], [13], [14], [22], [23] leverage large language models (LLMs) for flexible semantic reasoning, yet they overly depend on LLMs and LVLMs to generate semantic labels for 3D features without sufficient 3D scene awareness. This often results in inconsistent or inaccurate outputs where objects and relations misalign with actual 3D semantics. Additionally, some

LLM-based methods [3], [19], [24], [25] fine-tune on task-specific datasets, improving performance on those tasks but still restricting free-form queries and requiring substantial training resources. Our work utilizes a training-free, free-form querying framework that constructs a scene graph with accurate nodes and relations, aligns 3D instances with correct semantics for scene understanding.

2) *3D Scene Graphs*: The 3D Scene Graph (3DSG) represents scene semantics compactly, with nodes for objects and edges for their relationships [26]–[28]. Recent methods [29], [30] use 3DSG for 3D scene representations. These works [26], [31], [32], such as VL-SAT [31], construct scene graphs to model scene representations, but are constrained by the closed vocabularies from their training data, limiting their ability to support free-form semantic queries. More recent approaches like ConceptGraph [13] and BBQ [14] leverage LLMs to generate nodes and edges in scene graphs. However, their heavy reliance on LLM-generated outputs without incorporating 3D scene context often leads to inconsistent scene representations misaligned with actual 3D semantics. Our approach constructs a semantically consistent 3D scene graph by first obtaining complete and accurate free-form nodes, then aligning them with correct semantic labels.

III. METHOD

In this section, we propose FreeQ-Graph, a framework that enables free-form querying with (A) a 3D spatial scene graph with complete nodes and relations to support free-form query, (B) the semantic alignment module to align nodes with the consistent semantic label, and (C) a LLM-based CoT-reasoning for scene spatial querying, as shown in Fig. 2.

A. Problem Formulation

Given each 3D scene \mathbf{P} with multi-view posed RGB observations $\mathbf{I} = \{I_i\}_{i=1,\dots,M}$ as input, where M is the total number of images. The objective of free-form querying via 3D scene graph is to depict a semantic 3D scene graph $\mathbf{G} = (\mathbf{V}, \mathbf{E})$ as the 3D scene representation, where $\mathbf{V} = \{\mathbf{v}_j\}_{j=1,\dots,J}$ denote the set of 3D objects and edges $\mathbf{E} = \{\mathbf{e}_k\}_{k=1,\dots,K}$ represents the relation between them. \mathbf{G} constitutes a structured representation of the semantic content of the 3D scene. Based on this semantic representation of the 3D scene \mathbf{G} , during the reasoning phase, it interacts and queries with the query q and finally outputs a final target \mathbf{v} .

Nodes. For each object $\mathbf{v}_i \in \mathbf{V}$, we characterize it as $\mathbf{v}_i = \{\mathbf{p}_i, \mathbf{f}_i, \mathbf{c}_i, \mathbf{b}_i, n_i\}$, where $\mathbf{p}_i = \{\mathbf{x}_j\}_{j=1}^{N_i}$ is the pointcloud that contains N_i points \mathbf{x}_j , \mathbf{f}_i is the semantic feature, \mathbf{c}_i is the node caption, \mathbf{b}_i is the 3D bounding box, n_i is the id of the node. We denote the set of all object categories as \mathcal{V} .

Edges. For each pair of nodes $\mathbf{v}_i, \mathbf{v}_j$, we denote the edge $\mathbf{e}_{ij} = \{\mathbf{r}_{ij}, \mathbf{d}_{ij}\}$, where $\mathbf{r}_{ij} \in \mathbf{E}$ is the relation label that provides the underlying rationale, \mathbf{d}_{ij} is the Euclidean distance between centers of bounding boxes for \mathbf{v}_i and \mathbf{v}_j .

The construction of the object set \mathbf{V} and edge set \mathbf{E} is in Sec. III-B. For each object \mathbf{v}_i , we define the object-level information \mathbf{s}_{o_i} as $\mathbf{s}_{o_i} = \{\mathbf{c}_i, \mathbf{b}_i, n_i\}$. For better reasoning, we define scene-level information \mathbf{s}_c which represents the scene captions. The detailed reasoning algorithm is in Sec. III-D.

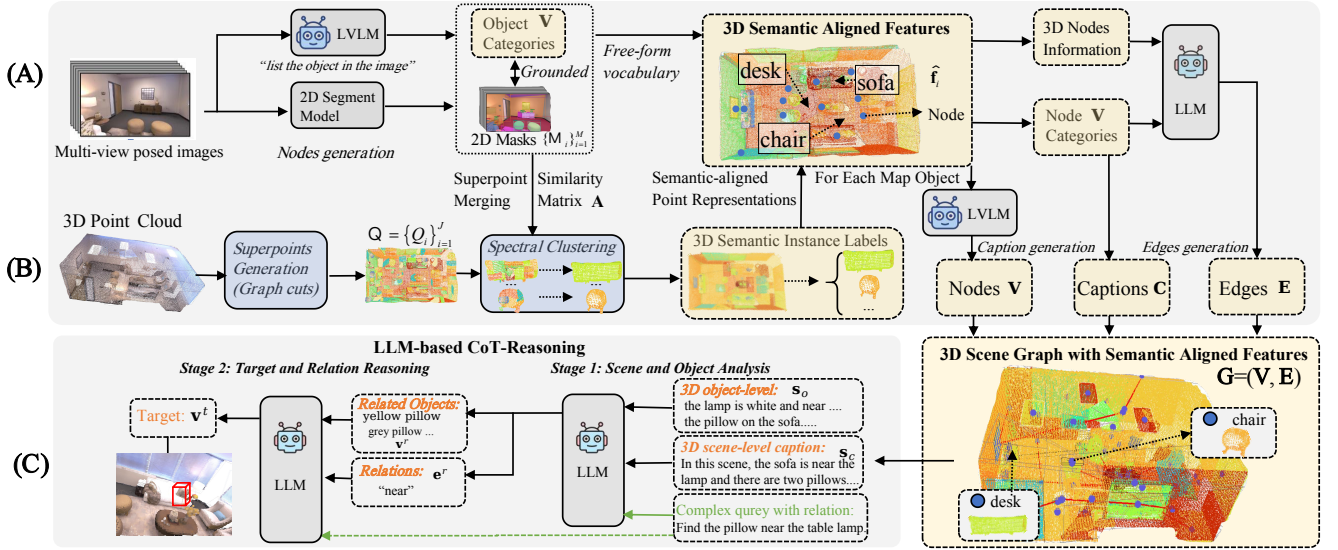


Fig. 2. The structure of FreeQ-Graph. We propose FreeQ-Graph to realize free-form semantic querying without any training priors for 3D scene understanding. (A) A 3D spatial scene graph to enable free-form semantic interaction with complete and accurate nodes and relations, (B) A semantic alignment module to align graph nodes with consistent semantic labels, and (C) An LLM-based CoT-reasoning algorithm for free-form semantic spatial querying.

B. 3D Scene Graph with Complete Nodes and Edges.

To facilitate the mapping of free-form objects and the capture of relations in 3D scenes, the crux lies in acquiring complete nodes, encompassing all small and thin objects, along with their complete captions, and edges that include detailed relations reflecting complex semantic connections. To achieve this, we construct the 3D scene graph G through three primary steps: 1) Complete and accurate nodes generation without any training priors. It is a free-form method without relying on predefined vocabulary. 2) 3D semantic consistent feature generation. 3) Edges and captions generation.

Complete 3D scene nodes generation without priors. To obtain objects with semantic labels without predefined vocabulary, we first adopt a large vision-language model (LVLM) [33] to obtain the object set, then use a 2D instance segmentation model [34] to correct potential hallucinations, forming the set \mathcal{V} of object categories, which can be denoted as:

$$\mathcal{V}, \{\mathcal{M}_i\}_{i=1}^M = \bigcup_{i=1}^M \phi(LVLM(I_i)) \quad (1)$$

where ϕ is the 2D segment model, \mathcal{M}_i is the mask set of image I_i . Specifically, for each 2D image view I_i , we prompt the LVLM model like “please list all the central objects in the scene, focus on smaller or overlooked objects, and visual attributes, omitting background details.” We use specific prompts to focus on smaller or overlooked objects. We then parse the response and obtain the initial object list for each image. To reduce potential hallucinations by the visual agent, we subsequently employ a 2D instance segmentation model [34] to ground all initial objects, identifying the final grounded object lists and obtaining the corresponding 2D object mask set $\{\mathcal{M}_i\}_{i=1}^M$, representing the candidate objects on the posed image I_i . We then construct the objects set \mathcal{V} by retaining categories from the combined set.

3D semantic consistent feature generation.

We extract visual descriptors (CLIP [7]) from 2D masks. Additionally, we generate 3D instance semantic labels via superpoint clustering and align nodes with point-level semantic representations (see Sec. III-C for details). The final nodes \mathbf{v}_i consist of point cloud \mathbf{p}_i , unit-normalized feature $\hat{\mathbf{f}}_i$, and 3D box \mathbf{b}_i .

3D nodes caption generation. For each posed image, building on ConceptGraph [13], we generate node captions via LVLM+LLM: (1) prompt LVLM with “describe the central object” at top- n clean viewpoints for initial descriptions; (2) distill coherent captions c_i via LLM refinement.

3D scene edges generation. Building upon 3D nodes and captions, we establish spatial edges through the 3D information analyzed by LLM. For each pair of nodes $\mathbf{v}_i, \mathbf{v}_j$, we compute pairwise similarity matrices via 3D bounding box IoU, then prune edges using Minimum Spanning Tree optimization. Next, we query LLMs with node captions/coordinates (e.g., “What is the relationship between 1 and 2?”) to extract spatial relations. We also calculate the Euclidean distance \mathbf{d}_{ij} between box centers. Thus we can generate the edge $\mathbf{e}_{ij} = \{\mathbf{r}_{ij}, \mathbf{d}_{ij}\}$.

C. 3D Scene Graph with Semantic Aligned Features

LLM-generated 3D scene graphs often suffer from potential inconsistencies with actual 3D semantics due to the lack of 3D scene information. This deficiency can lead to reasoning errors, such as misalignment between the semantic labels of 3D instance features and the nodes in the scene graph. To address this, we generate 3D semantic labels for instance features, ensuring precise alignment between each point and its corresponding semantics, thereby rectifying node-semantic misalignment. This alignment occurs in two key steps: (1) **3D semantic instance labels generation.** We apply graph cuts to segment the scene into superpoints, each superpoint represents a semantic label (e.g., “desk” or “chair”). Then we generate semantic labels through structural clustering for 3D instance

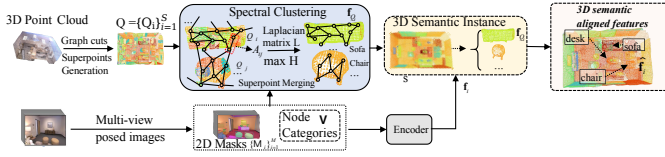


Fig. 3. Detailed process of 3D semantic instance label generation and semantic aligned features.

features and align the graph nodes with consistent semantic labels. **(2) 3D semantic-aligned feature representation.** We integrate visual features with superpoint-based semantic label features to produce the final semantic-aligned features.

3D semantic instance label generation. We aim to generate 3D semantic labels of nodes from superpoint merging. Specifically, as shown in Fig. 3, inspired by PoLo [35], we segment the 3D point cloud \mathbf{P} into S superpoints $\mathcal{Q} = \{Q_i\}_{i=1}^S$ using graph cuts, where each Q_i is a binary mask label of points. To merge superpoints into 3D instances, we construct a similarity matrix A , where each element A_{ij} represents the similarity between superpoints Q_i and Q_j :

$$A_{ij} = \left(\sum_{m=1}^M g(O_{i,m}, \tau_{\text{iou}}) \cdot g(O_{j,m}, \tau_{\text{iou}}) \right) \cdot \frac{f_{Q_i}^\top f_{Q_j}}{\|f_{Q_i}\| \|f_{Q_j}\|} \quad (2)$$

where $O_{i,m}$ and $O_{j,m}$ is the 2D mask projection of superpoint Q_i and Q_j in the m -th image. $g(O, \tau_{\text{iou}})$ is 1 if the IoU of mask O exceeds threshold τ_{iou} , and 0 otherwise. f_{Q_i} and f_{Q_j} are the semantic representations of Q_i and Q_j , obtained by encoding their label into feature vectors using a text encoder. We then perform spectral clustering by the Laplacian matrix L and segmenting superpoints via its eigenvectors. The optimal clustering dimension H is set using the eigengap heuristic, selecting H with the largest eigenvalue gap to determine the final number of superpoint semantic labels:

$$L = D^{-1/2}(D - A)D^{-1/2}, \quad H = \arg \max_{1 \leq j \leq J-2} (\lambda_{j+1} - \lambda_j) \quad (3)$$

where D is the degree matrix, with $D_{ii} = \sum_j A_{ij}$. λ_j are the eigenvalues of L , and the maximum gap corresponds to the optimal number of clusters.

3D semantic aligned features. After obtaining 3D semantic feature labels, we aim to align scene graph nodes with point-level semantic representations for 3D semantic aligned features. Unlike prior works [13], [14] that rely solely on a visual encoder for per-point representation, we employ both a vision encoder and a text encoder to ensure semantic consistency between nodes and point representations. Specifically, for each the node \mathbf{v}_i and its assigned semantic superpoint label Q_i , we first extract its visual feature \mathbf{f}_i using CLIP. Additionally, we encode the superpoint's semantic label Q_i through a encoder to obtain its semantic feature \mathbf{f}_{Q_i} , and fuse it with the visual feature via meanpooling φ to obtain the final semantically aligned representation $\hat{\mathbf{f}}_i$.

$$\hat{\mathbf{f}}_i = \varphi(\mathbf{f}_{Q_i}, \mathbf{f}_i) \quad (4)$$

where φ is the mean pooling. The $\hat{\mathbf{f}}_i$ is used to align semantic labels (e.g., “desk”) to nodes in the graph. Errors in LLMs and LVLMs may misassign labels of 3D instance features, leading to incorrect results in JSON-based reasoning.

D. LLM-based CoT-Reasoning

We designed the reasoning algorithm that breaks complex queries into CoT-reasoning, combining scene-level \mathbf{s}_c and object-level information \mathbf{s}_o (defined in Sec. III-A) for free-form semantic querying. Note that the CoT-reasoning are not separate. In the stage 1, we generate candidate objects, which are refined by further analysis in the next stage.

Stage 1: Scene and Object Analysis. As shown in Fig. 2 (C), to obtain the candidate targets \mathbf{v}_r and relations \mathbf{e}_r , we input the user’s complex query q alongside both object-level \mathbf{s}_o and scene-level information \mathbf{s}_c which defined in Sec. III-A into the LLM, which can be denoted as:

$$n_r, \mathbf{e}_r = \text{LLM}(q, \mathbf{s}_o, \mathbf{s}_c) \quad (5)$$

where n_r is IDs of candidate targets \mathbf{v}_r , scene-level information \mathbf{s}_c represents scene captions. This stage serves two purposes: 1) Leveraging the LLM’s planning ability to summarize observations of the entire scene, then decompose the complex semantic query into target and relational queries. 2) Cooperating object-level information with scene-level details, we aim to capture spatial relationships like “near” in Fig. 2 (C), without overlooking smaller or less prominent objects.

The LLM agent decomposes the user’s query into object and relation queries, identifying candidate ids of related targets. The “object query” refers to the primary candidate objects cited in the semantic query. The “relation query” identifies the relations of the candidate objects with the target, also providing the Euclidean distance of pairs.

Stage 2: Target and Relation Reasoning. We further leverage the LLM for spatial reasoning based on the candidate objects \mathbf{v}_r , relation \mathbf{e}_r , and the query q , then generate the final target \mathbf{v}^t . The reasoning stage can be denoted as:

$$\mathbf{v}^t = \text{LLM}(q, \mathbf{v}_r, \mathbf{e}_r) \quad (6)$$

With the candidate IDs, we input the corresponding objects’ captions, relations, 3D information, and the Euclidean distance from each candidate object to the centroid, along with the query q , into the LLM to infer the final target object.

IV. EXPERIMENT

A. Datasets and Implementation Details

1) Datasets: We evaluated on Sr3D [36] and Nr3D [36], and ScanRefer [37] for visual grounding, and scene segmentation task on Replica [38] and ScanNet [39] RGB-D. We validate the accuracy of scene graph on the 3DSSG dataset [28]. **Sr3D** [36] dataset includes annotations based on spatial relationships between objects, while **Nr3D** [36] consists of human-labeled language object references. We selected a subset of 526 objects from Sr3D and filtered queries in Nr3D that only involved spatial relations between objects. For 8 corresponding ScanNet scenes, we conducted relational queries in the format (target, relation, anchor). We evaluate on Nr3D and Sr3D’s standard splits using only the val set.

ScanRefer [37] comprises 51,583 descriptions for 11,046 objects across 800 ScanNet [39] scenes. Following the benchmark, the dataset is split into train/val/test sets with 36,655, 9,508, and 5,410 samples, using the val set for evaluation.

TABLE I
COMPARISONS OF 3D VISUAL GROUNDING ON SCANREFER [37] DATASET. THE ACCURACY AT 0.25 AND 0.5 IOU THRESHOLDS IS PRESENTED SEPARATELY FOR “UNIQUE,” “MULTIPLE,” AND “OVERALL” CATEGORIES.

| Method | Venue | Supervision | LLMs | Unique | | Multiple | | Overall | |
|--------------------|------------|-------------|--------------|--------------|--------------|--------------|--------------|--------------|--------------|
| | | | | Acc@0.25 | Acc@0.5 | Acc@0.25 | Acc@0.5 | Acc@0.25 | Acc@0.5 |
| ScanRefer [37] | ECCV'20 | Fully | - | 67.60 | 46.20 | 32.10 | 21.30 | 39.00 | 26.10 |
| InstanceRefer [17] | ICCV'21 | Fully | - | 77.50 | 66.80 | 31.30 | 24.80 | 40.20 | 32.90 |
| 3DVG-T [40] | ICCV'21 | Fully | - | 77.20 | 58.50 | 38.40 | 28.70 | 45.90 | 34.50 |
| BUTD-DETR [41] | ECCV'22 | Fully | - | 84.20 | 66.30 | 66.30 | 35.10 | 52.20 | 39.80 |
| EDA [18] | CVPR'23 | Fully | - | 85.80 | 68.60 | 49.10 | 37.60 | 54.60 | 42.30 |
| 3D-VisTA [6] | ICCV'23 | Fully | - | 81.60 | 75.10 | 43.70 | 39.10 | 50.60 | 45.80 |
| G3-LQ [42] | CVPR'24 | Fully | - | 88.60 | 73.30 | 50.20 | 39.70 | 56.00 | 44.70 |
| MCLN [43] | ECCV'24 | Fully | - | 86.90 | 72.70 | 52.00 | 40.80 | 57.20 | 45.70 |
| ConcreteNet [44] | ECCV'24 | Fully | - | 86.40 | 82.10 | 42.40 | 38.40 | 50.60 | 46.50 |
| 3DLFVG [45] | CVPR'24 | Fully | - | 65.80 | 51.27 | 22.03 | 16.94 | 30.53 | 23.61 |
| 3D-JCG [10] | CVPR'22 | Fully | - | 83.47 | 64.34 | 41.39 | 30.82 | 49.56 | 37.33 |
| Scene-Verse [11] | ECCV'24 | Fully | - | 81.60 | 75.10 | 43.70 | 39.10 | 50.60 | 45.80 |
| TSP3D [46] | CVPR'25 | Fully | - | - | - | - | - | 56.45 | 46.71 |
| LIBA [21] | AAAI'25 | Fully | - | 88.81 | 74.27 | 54.42 | 44.41 | 59.57 | 48.96 |
| WS-3DVG [47] | ICCV'23 | Weakly | - | - | - | - | - | 27.40 | 22.00 |
| OpenScene [3] | CVPR'23 | Fine-tuning | CLIP | 20.10 | 13.10 | 11.10 | 4.40 | 13.20 | 6.50 |
| Chat-3D v2 | NeurIPS'24 | Fine-tuning | Vicuna1.5-7B | 61.20 | 57.60 | 25.20 | 22.60 | 35.90 | 30.40 |
| ReGround3D [25] | ECCV'24 | Fine-tuning | FlanT5XL-3B | - | - | - | - | 55.50 | 50.20 |
| ChatScene [24] | NIPS'24 | Fine-tuning | Vicuna1.5-7B | - | - | - | - | 55.50 | 50.20 |
| Inst3D-LMM [19] | CVPR'25 | Fine-tuning | Vicuna1.5-7B | 88.60 | 81.50 | 48.70 | 43.20 | 57.80 | 51.60 |
| Open3DSG [32] | CVPR'24 | Zero-Shot | CLIP | 17.54 | 11.38 | 32.13 | - | - | 14.32 |
| LERF [48] | ICCV'23 | Zero-Shot | CLIP | - | - | - | - | 4.80 | 0.90 |
| ConceptGraphs [13] | ICRA'24 | Zero-Shot | GPT-4 | 16.50 | 10.32 | 9.57 | 7.69 | 13.28 | 9.31 |
| BBQ [14] | Arxiv'24 | Zero-Shot | GPT-4o | 19.40 | 11.60 | - | - | - | - |
| LLM-Grounder [6] | ICRA'24 | Zero-Shot | GPT-3.5 | - | - | - | - | 14.30 | 4.70 |
| LLM-Grounder [6] | ICRA'24 | Zero-Shot | GPT-4 turbo | - | - | - | - | 17.10 | 5.30 |
| ZSVG3D [49] | CVPR'24 | Zero-Shot | GPT-4 turbo | 63.80 | 58.40 | 27.70 | 24.60 | 36.40 | 32.70 |
| VLM-Grounder [22] | CoRL'24 | Zero-Shot | GPT-4o | 66.00 | 29.80 | 48.30 | 33.50 | 51.60 | 32.80 |
| SeeGround [23] | CVPR'25 | Zero-Shot | Qwen2-VL-72B | 75.70 | 68.90 | 34.00 | 30.00 | 44.10 | 39.40 |
| Ours | - | Zero-Shot | GPT-3.5 | 82.00 | 78.00 | 50.08 | 38.26 | 56.04 | 48.13 |
| Ours | - | Zero-Shot | GPT-4 | 82.10 | 78.70 | 50.82 | 37.98 | 55.46 | 48.86 |
| Ours | - | Zero-Shot | Vicuna1.5-7B | 82.04 | 78.31 | 49.18 | 38.42 | 55.97 | 48.72 |
| Ours | - | Zero-Shot | Qwen2-VL-72B | 83.10 | 79.40 | 50.16 | 39.13 | 56.13 | 49.41 |
| Ours | - | Zero-Shot | GPT-4 turbo | 82.50 | 79.00 | 50.96 | 39.08 | 55.73 | 49.04 |
| Ours | - | Zero-Shot | GPT-4o | 82.86 | 79.52 | 50.63 | 39.73 | 56.46 | 49.86 |

TABLE II
COMPARISONS OF 3D VISUAL GROUNDING ON SR3D [36] AND NR3D [36]. WE EVALUATE THE TOP-1 ACCURACY USING GROUND-TRUTH BOXES. “SUPER”: SUPERVISION METHOD.

| Method | Super | Nr3d | | | | | Sr3d | | | | |
|--------------------|-----------|-------------|-------------|-------------|-------------|-------------|-------------|-------------|-------------|-------------|-------------|
| | | Overall | Easy | Hard | V-Dep. | V-Indep | Overall | Easy | Hard | V-Dep. | V-Indep |
| InstanceRefer [17] | Fully | 38.8 | 46.0 | 31.8 | 34.5 | 41.9 | 48.0 | 51.1 | 40.5 | 45.8 | 48.1 |
| FFL-3DOG [50] | Fully | 41.7 | 48.2 | 35.0 | 37.1 | 44.7 | - | - | - | - | - |
| LAR [51] | Fully | 48.9 | 58.4 | 42.3 | 47.4 | 52.1 | 59.4 | 63.0 | 51.2 | 50.0 | 59.1 |
| SAT [52] | Fully | 56.5 | 64.9 | 48.4 | 54.4 | 57.6 | 57.9 | 61.2 | 50.0 | 49.2 | 58.3 |
| 3D-SPS [53] | Fully | 51.5 | 58.1 | 45.1 | 48.0 | 53.2 | 62.6 | 56.2 | 65.4 | 49.2 | 63.2 |
| 3DJCG [10] | Fully | 52.4 | 59.3 | 47.6 | 46.8 | 55.9 | 58.5 | 64.7 | 51.8 | 52.0 | 65.6 |
| BUTD-DETR [41] | Fully | 54.6 | 60.7 | 48.4 | 46.0 | 58.0 | 67.0 | 68.6 | 63.2 | 53.0 | 67.6 |
| MVT [54] | Fully | 59.5 | 67.4 | 52.7 | 59.1 | 60.3 | 64.5 | 66.9 | 58.8 | 58.4 | 58.4 |
| ViL3DRel [20] | Fully | 64.4 | 70.2 | 57.4 | 62.0 | 64.5 | 72.8 | 74.9 | 67.9 | 63.8 | 73.2 |
| EDA [18] | Fully | 52.1 | 58.2 | 46.1 | 50.2 | 53.1 | 68.1 | 70.3 | 62.9 | 54.1 | 68.7 |
| 3D-VisTA [6] | Fully | 64.2 | 72.1 | 56.7 | 61.5 | 65.1 | 76.4 | 78.8 | 71.3 | 58.9 | 77.3 |
| Scene-Verse [11] | Fully | 64.9 | 72.5 | 57.8 | 56.9 | 67.9 | 77.5 | 80.1 | 71.6 | 62.8 | 78.2 |
| TSP3D | Fully | 48.7 | - | - | - | - | 57.1 | - | - | - | - |
| MPEC | Fully | 66.7 | - | - | - | - | 80.0 | - | - | - | - |
| WS-3DVG [55] | Weakly | 27.3 | 18.0 | 21.6 | 22.9 | 22.5 | - | - | - | - | - |
| ZSVG3D [49] | Zero-Shot | 46.5 | 31.7 | 36.8 | 40.0 | 39.0 | - | - | - | - | - |
| SeeGround [23] | Zero-Shot | 54.5 | 38.3 | 42.3 | 48.2 | 46.1 | - | - | - | - | - |
| ConceptGraph* [13] | Zero-Shot | 38.2 | 39.4 | 32.6 | 42.1 | 38.7 | 43.6 | 44.3 | 41.9 | 38.4 | 49.7 |
| BBQ* [14] | Zero-Shot | 45.0 | 47.6 | 41.2 | 46.3 | 45.0 | 49.9 | 53.9 | 49.3 | 45.6 | 50.7 |
| VLM-Grounder [22] | Zero-Shot | 48.0 | 55.2 | 39.5 | 45.8 | 49.4 | - | - | - | - | - |
| SORT3D [56] | Zero-Shot | 60.5 | - | - | 56.6 | 62.3 | - | - | - | - | - |
| CSVG [57] | Zero-Shot | 59.2 | - | - | 53.0 | 62.5 | - | - | - | - | - |
| Ours | Zero-Shot | 61.8 | 61.4 | 57.8 | 60.9 | 67.1 | 70.9 | 79.3 | 63.9 | 64.1 | 76.5 |

Replica [38] is a dataset of 18 realistic 3D indoor scene reconstructions, covering rooms to buildings. We selected 8 scene data samples (room0, room1, room2, office0, office1, office2, office3, office4) with their annotations.

ScanNet [39] is an instance-level indoor RGB-D dataset containing both 2D and 3D data. We selected 8 scene samples, which are 0011, 0030, 0046, 0086, 0222, 0378, 0389, 0435.

3DSSG dataset [28] offers annotated 3D semantic scene graphs. Adopting the RIO27 annotation, we evaluate 27 classes and 16 relationship classes and adhere to the experimental

protocol of EdgeGCN [58] for the fair comparison, dividing the dataset into train/val/test sets with 1084/113/113 scenes. All the camera viewpoints follow the original dataset settings.

2) *Performance Metric*: For visual grounding on the Sr3D [36] and Nr3D [36], we follow the ReferIt3D [36] protocol by using ground-truth object masks and measuring grounding accuracy, whether the model correctly identifies the target object among the ground-truth proposals. Additionally, to ensure a fair comparison with related works [13], [14], [32], we also report Acc@0.1 IoU and Acc@0.25 IoU for the “easy”, “hard”, “view-dep.” and “view-indep.” cases. For ScanRefer [37], we calculate the metrics including Acc@0.25 IoU and Acc@0.5 IoU, reported for both unique, multiple, and overall categories. “Unique” which refers to scenes containing only one target object, “Multiple” which includes scenes with distractor objects from the same class, and “Overall” which represents the aggregated results across all scene categories. For Replica [38] and ScanNet [39], We compute the metrics of mAcc, mIoU, and fmIoU. For 3DSSG [28], we adopt the widely used top-k recall metric (R@k) for scene graph evaluation, assessing objects, predicates, and relationships separately. For assessment, as shown in Table V, Recall@5 and Recall@10 are used for object classification, Recall@3 and Recall@5 for predicate classification, and Recall@50 and Recall@100 for relationship classification. For out-of-word queries, we validate results using manually annotated ground truth, which will be publicly available. For 5 tested datasets, we all follow the original queries and annotations.

3) *Implementation Details*: We conduct experiments on the NVIDIA 3090 GPU using PyTorch. We adopt GPT-4o [8] as the LLM, LLaVa-7B-v1.6 [33] as the LVLM. For 2D objects

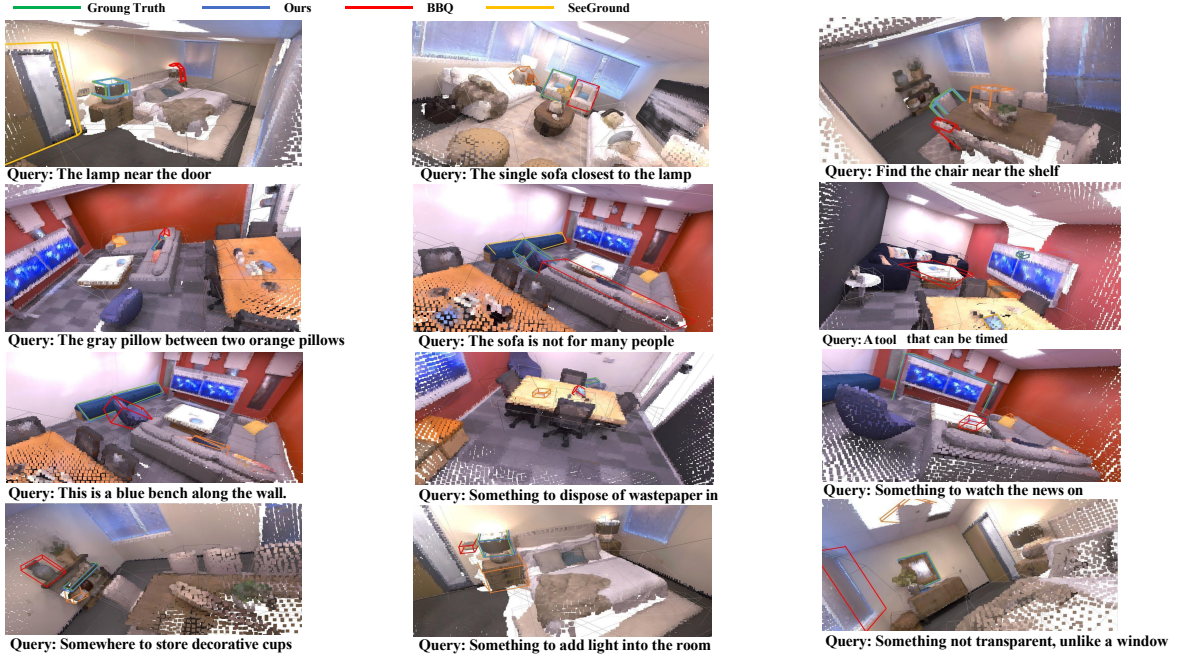


Fig. 4. Comparison of 3D object visual grounding task with free-form query. The ground truth box is in green.

TABLE III
COMPARISONS OF 3D VISUAL GROUNDING ON Sr3D [36] AND Nr3D [36] DATASETS. THE ACCURACY (A) AT 0.1 AND 0.25 IOU THRESHOLDS IS PRESENTED SEPARATELY FOR 5 CATEGORIES.

| Methods | Sr3D | | | | | | | | | | Nr3D | | | | | | | | | |
|-------------------|-------------|-------------|-------------|-------------|-------------|-------------|-------------|-------------|-------------|-------------|-------------|-------------|-------------|-------------|-------------|-------------|-------------|-------------|-------------|-------------|
| | Overall | | Easy | | Hard | | View Dep. | | View Indep. | | Overall | | Easy | | Hard | | View Dep. | | View Indep. | |
| | A@0.1 | A@0.25 | A@0.1 | A@0.25 | A@0.1 | A@0.25 | A@0.1 | A@0.25 | A@0.1 | A@0.25 | A@0.1 | A@0.25 | A@0.1 | A@0.25 | A@0.1 | A@0.25 | A@0.1 | A@0.25 | A@0.1 | A@0.25 |
| OpenFusion [45] | 12.6 | 2.4 | 14.0 | 2.4 | 1.3 | 1.3 | 3.8 | 2.5 | 13.7 | 2.4 | 10.7 | 1.4 | 12.9 | 1.4 | 5.1 | 1.5 | 8.5 | 0.0 | 11.4 | 1.9 |
| ConceptGraph [13] | 13.3 | 6.2 | 13.0 | 6.8 | 16.0 | 1.3 | 15.2 | 5.1 | 13.1 | 6.4 | 16.0 | 7.2 | 18.7 | 9.2 | 9.1 | 2.0 | 12.7 | 4.2 | 17.0 | 8.1 |
| BBQ [14] | 34.2 | 22.7 | 34.3 | 22.7 | 33.3 | 22.7 | 32.9 | 20.3 | 34.4 | 23.0 | 28.3 | 19.0 | 30.5 | 21.3 | 22.8 | 13.2 | 23.6 | 18.2 | 29.8 | 19.3 |
| Open3DSG [32] | 37.3 | 25.8 | 36.5 | 24.8 | 36.1 | 25.9 | 36.1 | 23.2 | 36.6 | 25.3 | 31.4 | 22.5 | 32.3 | 24.3 | 25.2 | 16.8 | 24.3 | 21.2 | 33.5 | 22.8 |
| 3DLFGV [45] | - | 18.3 | - | 15.1 | - | 19.0 | - | 18.3 | - | 22.4 | - | 19.3 | - | 21.0 | - | 15.2 | - | 11.2 | - | 19.1 |
| Ours | 61.1 | 46.3 | 60.8 | 46.4 | 57.8 | 54.9 | 59.3 | 51.2 | 60.9 | 52.6 | 51.3 | 43.5 | 58.2 | 45.9 | 47.4 | 39.8 | 50.3 | 47.6 | 54.3 | 38.9 |

and encoding, we use Grounded-SAM [34] for 2d mask segmentation and employ the CLIP ViT-L/14 encoder [59] as the visual feature extractor. We select the top-5 view masks with the highest projected point IoU for each superpoint. Following ConceptGraph [13], for each object, we select relevant image crops from the Top-10 best views and pass them to LLM to generate captions. For superpoint merging, we employ consistent thresholds of $\tau_{iou} = 0.9$ and $\tau_{sim} = 0.9$ across all experiments. For each superpoint, we select the top-5 view masks with the highest IoU relative to the projected points. Following ConceptGraph [13], we set the voxel size and nearest neighbor threshold to 2.5 cm, and use an association threshold of 1.1.

B. Experiment Results

1) *3D Object Grounding*: We conducted 3D visual grounding comparisons on the Nr3D [36], Sr3D [36], and ScanRefer [37] datasets. As shown in Table I, we conducted comprehensive experimental comparisons on the ScanRefer [37] benchmark, evaluating a wide range of models across different learning paradigms. These include state-of-the-art fully supervised approaches [6], [10]–[12], [17], [40], [41], [60], weakly supervised methods [55], fine-tuned models [3], [19],

[24], [25] refer to methods that are adapted to specific tasks after fine-tuning, and zero-shot approaches [3], [6], [13], [14], [23], [32], [48] refer to methods that directly use LLMs without fine-tuning. Our model, without requiring any training, achieved best results, fully demonstrating its superiority. While our training-free model does not surpass fully-supervised or fine-tuned approaches like Scene-Verse [11] and Inst3D-LLM [19], which demand extensive training on 3D data and LLMs, it achieves comparable performance without any training cost, underscoring its efficiency and effectiveness. Furthermore, compared to the zero-shot models, our model achieved best results across all categories with a clear advantage. To further substantiate our findings, we also performed ablation experiments on different LLM agents, which further demonstrates that our model consistently yields optimal results across various LLMs.

Besides, for Sr3D and Nr3D datasets, we evaluate the top-1 using ground-truth boxes in Table II and the accuracy at 0.1 and 0.25 IOU threshold for 5 categories in Table III. As shown in Table II, we validated the top-1 performance using ground-truth boxes across fully-supervised models [6], [10], [17], weakly-supervised model [55], and zero-shot models [23], [49]. Our model achieved best results across 5 different metrics, demonstrating its superior performance. As shown

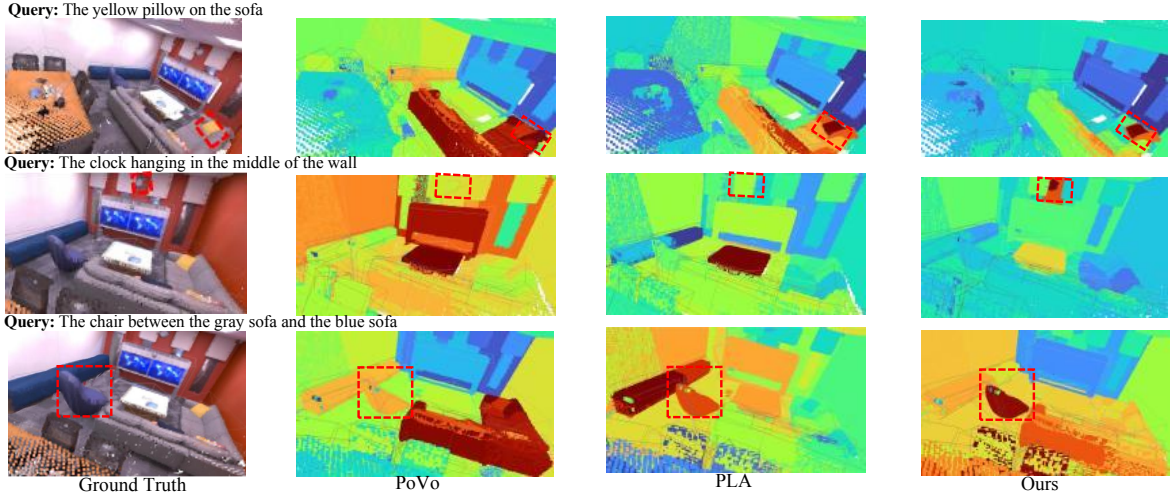


Fig. 5. Comparison semantic segmentation on the Replica dataset. The semantic map highlights the regions most relevant to the query’s semantic features, with deeper colors indicating higher relevance, where red represents the most relevant semantics.

TABLE IV

COMPARISONS OF 3D SEMANTIC SEGMENTATION TASK BETWEEN OUR MODEL AND SOTA METHODS ON REPLICA AND SCANNet DATASETS.

| Method | Type | Replica | | | ScanNet | | |
|--------------------|------------|-------------|-------------|-------------|-------------|-------------|-------------|
| | | mAcc↑ | mIoU↑ | fmIoU↑ | mAcc↑ | mIoU↑ | fmIoU↑ |
| LSeg [61] | Privileged | 0.33 | - | 0.40 | - | - | - |
| OpenSeg [62] | | 0.41 | - | 0.54 | - | - | - |
| OpenFusion [63] | | 0.41 | 0.30 | 0.58 | 0.67 | 0.53 | 0.64 |
| OpenScene [3] | | - | - | - | 0.69 | - | 0.58 |
| MPEC [64] | Zero-shot | - | - | - | 0.79 | - | 0.65 |
| Mask2former [65] | | 0.05 | - | 0.01 | - | - | - |
| ConceptFusion [66] | | 0.29 | 0.11 | 0.14 | 0.49 | 0.26 | 0.31 |
| OpenMask3D [67] | | - | - | - | 0.34 | 0.18 | 0.20 |
| ConceptGraphs [13] | Zero-shot | 0.36 | 0.18 | 0.15 | 0.52 | 0.26 | 0.29 |
| HOV-SG [68] | | 0.29 | 0.23 | - | 0.44 | 0.22 | 0.29 |
| BBQ-CLIP [14] | | 0.38 | 0.27 | 0.48 | 0.56 | 0.34 | 0.36 |
| Open3DSG [32] | | 0.35 | 0.31 | 0.45 | 0.52 | 0.36 | 0.31 |
| PoVo [35] | Zero-shot | 0.34 | 0.35 | 0.52 | 0.34 | 0.39 | 0.36 |
| PLA [4] | | - | - | - | 0.41 | - | 0.19 |
| Ours | | 0.49 | 0.42 | 0.66 | 0.82 | 0.57 | 0.69 |

in Table III, our model also consistently outperformed all SOTA works [13], [14], [63] across 4 cases of Sr3D and Nr3D datasets. Compared to ConceptGraph [13], BBQ [14] and Open3DSG [32], which also utilize LLMs and graph representations for reasoning, our model shows significant advantages, validating the semantic aligned features in reasoning with free-form queries. Fig.4 shows the quantitative comparison. SeeGround [23] fails to capture object relationships like “near”, while BBQ [14] struggles with semantic label like “single sofa”, hindering accurate grounding. In contrast, our model precisely grounds objects with correct semantic labels and understands both scene-level and object-level spatial relationships.

2) *Complex Queries*: To evaluate our model’s capability for complex semantic queries, we compare the “hard” case on Sr3D [36] and Nr3D [36] datasets, and “Multiple” case on ScanRefer [37]. As shown in Tables III and I, our model exhibits significant advantages in handling all complex semantic queries and multi-object queries. This validates that our approach can more effectively comprehend complex semantic queries, leveraging 3D semantically consistent scene graphs.

TABLE V

COMPARISONS OF 3D SCENE GRAPH GENERATION IN OBJECT, PREDICATE, AND RELATIONSHIP PREDICTION ON 3DSSG [28] DATASET.

| Method | Object | | Predicate | | Relationship | |
|----------------------------------|-------------|-------------|-------------|-------------|--------------|-------------|
| | R@5 | R@10 | R@5 | R@10 | R@50 | R@100 |
| <i>Fully-supervised</i> | | | | | | |
| 3DSSG [28] | 0.68 | 0.78 | 0.89 | 0.93 | 0.40 | 0.66 |
| SGFN [60] | 0.70 | 0.80 | 0.97 | 0.99 | 0.85 | 0.87 |
| SGRec3D [12] | 0.80 | 0.87 | 0.97 | 0.99 | 0.89 | 0.91 |
| SGPN [28] | 0.68 | 0.78 | 0.89 | 0.93 | 0.40 | 0.66 |
| VL-SAT [31] | 0.78 | 0.86 | 0.98 | 0.99 | 0.90 | 0.93 |
| <i>Zero-shot open-vocabulary</i> | | | | | | |
| OpenSeg [62] | 0.38 | 0.45 | 0.10 | 0.23 | 0.05 | 0.07 |
| ConceptGraphs [13] | 0.41 | 0.48 | 0.39 | 0.47 | 0.32 | 0.28 |
| BBQ [14] | 0.43 | 0.54 | 0.46 | 0.54 | 0.41 | 0.42 |
| Open3DSG [32] | 0.57 | 0.68 | 0.63 | 0.70 | 0.64 | 0.66 |
| Ours | 0.69 | 0.78 | 0.74 | 0.84 | 0.72 | 0.78 |

As illustrated in rows 3-4 of Fig. 4, we further present a comparison of our model against BBQ [14] and SeeGround [23] in 3D visual grounding with complex free-form semantic queries. The results demonstrate that our model consistently identifies the correct target objects under various complex semantic queries, whereas others struggle to comprehend and resolve such intricate semantics.

3) *3D Semantic Segmentation*: As shown in Table IV and Fig. 5, we evaluate on 3D semantic segmentation task on Replica [38] and ScanNet [39] datasets. Following ConceptGraph [13], we matched object nodes’ fused features to CLIP text embeddings of “an image of class”, then assigned points to their semantic categories via similarity scores. We compare our model against SOTA zero-shot 3D open-vocabulary segmentation methods [13], [14], [65]–[67] and privileged approaches leveraging pre-trained datasets [45], [61], [62], where our method consistently achieves notable gains. Compared to BBQ [14] and Open3DSG [32], our model delivers superior results on the ScanNet benchmark [39]. Furthermore, our zero-shot approach surpasses OpenFusion [63], a supervised model fine-tuned for semantic segmentation, highlighting the strength of our training-free framework. In Fig. 5, following ConceptGraph [13], we compute the similarity between each

TABLE VI
ABLATION STUDY. GRAPH: 3D SCENE GRAPH, SA: SEMANTIC ALIGNMENT. REASONING: LLM-BASED REASONING. WE PRESENT THE OVERALL ACCURACY.

| Method | | | Sr3D | | Nr3D | |
|--------|----|-----------|---------|----------|---------|----------|
| Graph | SA | Reasoning | Acc@0.1 | Acc@0.25 | Acc@0.1 | Acc@0.25 |
| × | × | × | 13.3 | 6.2 | 16.0 | 7.2 |
| ✓ | × | × | 33.7 | 21.2 | 29.7 | 21.1 |
| ✓ | ✓ | × | 43.3 | 32.2 | 38.9 | 30.3 |
| ✓ | ✓ | ✓ | 61.1 | 46.3 | 51.3 | 43.5 |

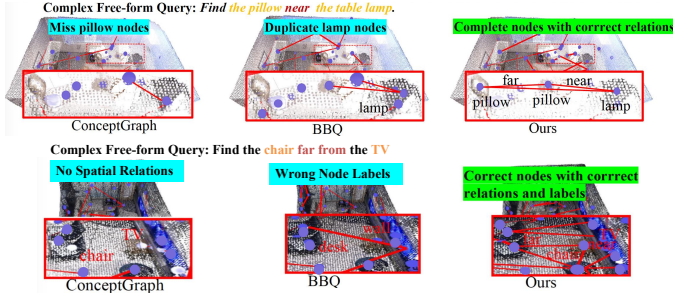


Fig. 6. Comparison of our semantic consistent scene graph with other scene graphs of the ConceptGraph [13] and BBQ [14].

node’s semantic features and the query’s CLIP text embedding, with darker map colors (red) indicating higher semantic similarity. Our method pinpoints key semantic features, whereas others fixate on irrelevant cues. For various free-form semantic queries, our model accurately segments the corresponding semantic areas, while PoVo [35] and PLA [4] fail to understand these complex, free-form semantic queries.

4) *3D Scene Graph*: Table V shows our 3D scene graph evaluation on 3DSSG [28], where we surpass all SOTA models [13], [14], [32], [62] in object, predicate, and relationship prediction. This demonstrates that methods leverage on pre-train datasets, such as OpenSeg [62], are unsuitable for predicting object nodes and relationships, while models over-rely on LLMs (e.g., ConceptGraph [13], BBQ [14]) fail on small or thin objects. While Open3DSG [32] can predict open-vocabulary objects, it still faces challenges in free-form relationship prediction. In contrast, our model can precisely predict free-form objects, predicates, and relationships without any training priors. As shown in Fig 6, it illustrates that our model not only creates a semantically consistent scene graph with complete nodes and correct relations but also assigns the correct semantic labels to each node.

C. Ablation Study

Ablations are conducted to validate the efficacy of the proposed methods. In the first row of Table 5, we use ConceptGraph [13] as a baseline. For the model without reasoning, we apply ConceptGraph’s simpler reasoning for inference.

1) *3D Scene Graph*: The comparison between Rows 1–2 in Table VI demonstrates that our 3D scene graph significantly improves visual grounding performance on Sr3D and Nr3D. This validates the effectiveness of our scene representation in capturing free-form objects and their relationships. As illustrated in Fig. 6, our model constructs a semantically consistent scene graph with complete nodes and accurate relations.

TABLE VII
COMPARISONS OF REASONING ALGORITHM ON SR3D AND NR3D.

| Method | Scene Reasoning | Edges | Sr3D | | Nr3D | |
|--------------------|------------------|----------|-------------|-------------|-------------|-------------|
| | | | Acc@0.1 | Acc@0.25 | Acc@0.1 | Acc@0.25 |
| BBQ [14] | Random | - | 0.02 | 0.01 | 0.02 | 0.01 |
| Ours | Random | - | 0.21 | 0.13 | 0.16 | 0.14 |
| ConceptGraphs [13] | ConceptGraphs | - | 0.08 | 0.02 | 0.07 | 0.03 |
| ConceptGraphs [13] | BBQ | distance | 0.15 | 0.08 | 0.12 | 0.08 |
| ConceptGraphs [13] | Ours (two-stage) | distance | 0.36 | 0.27 | 0.33 | 0.29 |
| BBQ [14] | Deductive | distance | 0.34 | 0.23 | 0.28 | 0.19 |
| BBQ [14] | ConceptGraphs | distance | 0.30 | 0.19 | 0.25 | 0.13 |
| BBQ [14] | Ours (two-stage) | distance | 0.45 | 0.28 | 0.37 | 0.23 |
| Ours | Ours (two-stage) | distance | 0.61 | 0.46 | 0.51 | 0.44 |

TABLE VIII
COMPARISON OF MEAN AND OVERALL COMPUTATIONAL TIME.

| Methods | Replica (average) | | Nr3d (average) | | Sr3d (average) | | ScanRefer (avg) | |
|--------------|-------------------|--------------|----------------|------------|----------------|------------|-----------------|------------|
| | mean(s/it) | overall(min) | mean overall | | mean overall | | mean overall | |
| ConceptGraph | 3.56 | 24.6 | 3.98 | 25.8 | 3.71 | 23.4 | 4.13 | 27.6 |
| BBQ | 1.18 | 7.9 | 1.24 | 8.3 | 1.13 | 7.6 | 1.45 | 9.3 |
| Ours | 1.03 | 5.6 | 1.07 | 6.4 | 1.08 | 5.8 | 1.16 | 6.4 |

TABLE IX
ABLATION STUDIES OF DIFFERENT LLAVA MODELS.

| Method | LLava type | Sr3D | | Nr3D | |
|--------------------|----------------------|-------------|-------------|-------------|-------------|
| | | Acc@0.1 | Acc@0.25 | Acc@0.1 | Acc@0.25 |
| ConceptGraphs [13] | LLava-7b-v0 | 13.3 | 6.2 | 16.0 | 7.2 |
| | LLava-7b-v1.5 | 16.9 | 9.4 | 24.9 | 15.4 |
| | LLava-7b-v1.6 | 18.4 | 12.8 | 27.2 | 17.7 |
| BBQ [14] | LLava-7b-v0 | 27.2 | 17.9 | 31.4 | 26.3 |
| | LLava-7b-v1.5 | 31.7 | 20.3 | 39.5 | 30.6 |
| | LLava-7b-v1.6 | 34.2 | 22.7 | 41.3 | 33.5 |
| Ours | LLava-7b-v0 | 60.2 | 45.4 | 50.6 | 42.1 |
| | LLava-7b-v1.5 | 60.9 | 46.0 | 51.1 | 42.8 |
| | LLava-7b-v1.6 | 61.1 | 46.3 | 51.3 | 43.5 |

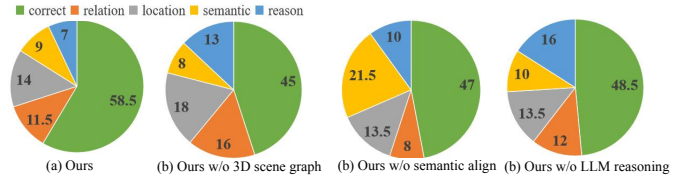


Fig. 7. Error analysis of FreeQ-Graph on ScanRefer dataset.

2) *Semantic Alignment*: As shown in rows 2 and 3 of Table VI, Aligning the semantic features of the graph nodes with the semantic consistent superpoint features significantly enhances the performance of two datasets. This highlights that the proposed module effectively aligns the consistent semantic label of the graph nodes, as shown in Fig. 6.

3) *LLM-based CoT-reasoning*: Rows 3–4 in Table VI show that the LLM-based reasoning enhances the model’s ability to infer complex semantics. It indicates that integrating scene-level and object-level information fosters a more nuanced understanding of complex scenes. Furthermore, by decomposing the complex query into two stages, the model more effectively identifies candidate objects and their relationships, enabling deeper analysis to determine the final target.

4) *Reasoning algorithms*: We explored how reasoning algorithms affect 3D object grounding on the Sr3D [36] and Nr3D [36], evaluating with Acc@0.1 and Acc@0.25 metrics. As shown in Table VII, our model outperforms various SOTA reasoning methods, models [13], [14]. Moreover, our reasoning algorithm can seamlessly integrate with others, such as ConceptGraph [13], significantly enhancing their ability to

handle free-form complex semantic queries. It demonstrates the superiority of our LLM-based reasoning algorithm for free-form scene semantic queries.

5) *Computational costs*: As shown in Table VIII, our method achieves superior efficiency with significantly lower computational cost than other zero-shot, LLM-based approaches that require no pre-training or fine-tuning [13], [14]. Unlike fully-supervised or fine-tuned LLM-based models that demand hours of training, our training-free framework highlights strong practical efficiency. While we also use a GPT-based model for reasoning, like ConceptGraph and BBQ, our method delivers faster inference under the same settings. This is enabled by our semantically aligned 3D scene graph, which ensures accurate and efficient semantic representation and relation extraction. Furthermore, our CoT reasoning decomposes complex queries into manageable steps, improving reasoning speed. In contrast, ConceptGraph and BBQ rely solely on LLM outputs, often overlooking inconsistencies that lead to semantic misalignment and slower performance.

6) *Error Analysis*: To assess reliance, we perform an error analysis on 200 randomly selected ScanRefer [37] samples (Fig. 7), categorizing errors into 5 cases. Our scene graph enhances localization and relation detection, while semantic alignment reduces mislabeling errors. Our reasoning module effectively mitigates inference errors and keep stability.

7) *Different LLaVA models.*: As shown in Table IX, ablation on different LLaVAs over Nr3D and Sr3D shows that advanced LLaVA improves grounding by reducing caption errors. Our model remains more stable than BBQ and ConceptGraph, indicating that our semantically consistent 3D scene graph and reasoning reduce reliance on specific versions.

V. CONCLUSION

In this paper, we propose FreeQ-Graph, which enables free-form querying for 3D scene understanding. The main contribution lies in semantically consistent 3D scene graphs, which capture 3D semantic-aligned features. Besides, we develop a LLM-based analysis and reasoning algorithm for free-form semantic querying. Experiments on 6 datasets show that our model excels in free-form queries and relational reasoning. Codes and datasets will be released.

Limitations. We consider potential limitations: 1) The use of multiple LLM and LVLM agents may increase inference time and costs. 2) Node captions are prone to errors due to the inherent limitations of current LVLMs.

REFERENCES

- [1] K. Liu, F. Zhan, J. Zhang, M. Xu, Y. Yu, A. El Saddik, C. Theobalt, E. Xing, and S. Lu, "3d open-vocabulary segmentation with foundation models," *arXiv preprint arXiv:2305.14093*, vol. 2, no. 3, p. 6, 2023.
- [2] R. Ding, J. Yang, C. Xue, W. Zhang, S. Bai, and X. Qi, "Lowis3d: Language-driven open-world instance-level 3d scene understanding," *IEEE Transactions on Pattern Analysis and Machine Intelligence*, 2024.
- [3] S. Peng, K. Genova, C. Jiang, A. Tagliasacchi, M. Pollefeys, T. Funkhouser *et al.*, "Openscene: 3d scene understanding with open vocabularies," in *Proc. Computer Vision and Pattern Recognition*, 2023, pp. 815–824.
- [4] R. Ding, J. Yang, C. Xue, W. Zhang, S. Bai, and X. Qi, "Pla: Language-driven open-vocabulary 3d scene understanding," in *Proc. Computer Vision and Pattern Recognition*, 2023, pp. 7010–7019.
- [5] N. M. M. Shafullah, C. Paxton, L. Pinto, S. Chintala, and A. Szlam, "Clip-fields: Weakly supervised semantic fields for robotic memory," *arXiv preprint arXiv:2210.05663*, 2022.
- [6] J. Yang, X. Chen, S. Qian, N. Madaan, M. Iyengar, D. F. Fouhey, and J. Chai, "Llm-grounder: Open-vocabulary 3d visual grounding with large language model as an agent," 2023. [Online]. Available: <https://arxiv.org/abs/2309.12311>
- [7] J. Zhang, R. Dong, and K. Ma, "Clip-fo3d: Learning free open-world 3d scene representations from 2d dense clip," in *Proc. of the IEEE/CVF International Conference on Computer Vision*, 2023, pp. 2048–2059.
- [8] J. Achiam, S. Adler, S. Agarwal, L. Ahmad, I. Akkaya, F. L. Aleman, D. Almeida, J. Altenschmidt, S. Altman, S. Anadkat *et al.*, "Gpt-4 technical report," *arXiv preprint arXiv:2303.08774*, 2023.
- [9] R. Fu, J. Liu, X. Chen, Y. Nie, and W. Xiong, "Scene-llm: Extending language model for 3d visual understanding and reasoning," *arXiv preprint arXiv:2403.11401*, 2024.
- [10] D. Cai, L. Zhao, J. Zhang, L. Sheng, and D. Xu, "3djcg: A unified framework for joint dense captioning and visual grounding on 3d point clouds," in *Proc. Computer Vision and Pattern Recognition*, 2022, pp. 16464–16473.
- [11] B. Jia, Y. Chen, H. Yu, Y. Wang, X. Niu, T. Liu, Q. Li, and S. Huang, "Scenaverse: Scaling 3d vision-language learning for grounded scene understanding," in *European Conference on Computer Vision*. Springer, 2024, pp. 289–310.
- [12] S. Koch, P. Hermosilla, N. Vaskevicius, M. Colosi, and T. Ropinski, "Sgrec3d: Self-supervised 3d scene graph learning via object-level scene reconstruction," 2023. [Online]. Available: <https://arxiv.org/abs/2309.15702>
- [13] Q. Gu, A. Kuwajerwala, S. Morin, K. M. Jatavallabhula, B. Sen, A. Agarwal, C. Rivera, W. Paul, K. Ellis, R. Chellappa, C. Gan, C. M. de Melo, J. B. Tenenbaum, A. Torralba, F. Shkurti, and L. Paull, "Conceptgraphs: Open-vocabulary 3d scene graphs for perception and planning," 2023. [Online]. Available: <https://arxiv.org/abs/2309.16650>
- [14] S. Linok, T. Zemskova, S. Ladanova, R. Titkov, D. Yudin, M. Monastyrny, and A. Valenkov, "Beyond bare queries: Open-vocabulary object grounding with 3d scene graph," 2024. [Online]. Available: <https://arxiv.org/abs/2406.07113>
- [15] Y. Yin, Y. Liu, Y. Xiao, D. Cohen-Or, J. Huang, and B. Chen, "Sai3d: Segment any instance in 3d scenes," in *Proc. Computer Vision and Pattern Recognition*, 2024, pp. 3292–3302.
- [16] P. Nguyen, T. D. Ngo, E. Kalogerakis, C. Gan, A. Tran, C. Pham, and K. Nguyen, "Open3dis: Open-vocabulary 3d instance segmentation with 2d mask guidance," in *Proc. Computer Vision and Pattern Recognition*, 2024, pp. 4018–4028.
- [17] Z. Yuan, X. Yan, Y. Liao, R. Zhang, S. Wang, Z. Li, and S. Cui, "Instancerefer: Cooperative holistic understanding for visual grounding on point clouds through instance multi-level contextual referring," in *Proc. of the IEEE/CVF International Conference on Computer Vision*, 2021, pp. 1791–1800.
- [18] Y. Wu, X. Cheng, R. Zhang, Z. Cheng, and J. Zhang, "Eda: Explicit text-decoupling and dense alignment for 3d visual grounding," in *Proc. Computer Vision and Pattern Recognition*, 2023, pp. 19231–19242.
- [19] H. Yu, W. Li, S. Wang, J. Chen, and J. Zhu, "Inst3d-Imm: Instance-aware 3d scene understanding with multi-modal instruction tuning," in *Proc. Computer Vision and Pattern Recognition*, 2025, pp. 14147–14157.
- [20] S. Chen, P.-L. Guhur, M. Tapaswi, C. Schmid, and I. Laptev, "Language conditioned spatial relation reasoning for 3d object grounding," *Advances in neural information processing systems*, vol. 35, pp. 20522–20535, 2022.
- [21] Y. Wang, Y.-L. Li, W. E. ZY, and S. Wang, "Liba: Language instructed multi-granularity bridge assistant for 3d visual grounding," in *Proceedings of the AAAI Conference on Artificial Intelligence*, vol. 39, no. 8, 2025, pp. 8114–8122.
- [22] R. Xu, Z. Huang, T. Wang, Y. Chen, J. Pang, and D. Lin, "Vlm-grounder: A vlm agent for zero-shot 3d visual grounding," *arXiv preprint arXiv:2410.13860*, 2024.
- [23] R. Li, S. Li, L. Kong, X. Yang, and J. Liang, "Seeground: See and ground for zero-shot open-vocabulary 3d visual grounding," in *Proc. Computer Vision and Pattern Recognition*, 2025.
- [24] H. Huang, Y. Chen, Z. Wang, R. Huang, R. Xu, T. Wang, L. Liu, X. Cheng, Y. Zhao, J. Pang *et al.*, "Chat-scene: Bridging 3d scene and large language models with object identifiers," *Proceedings of the Advances in Neural Information Processing Systems, Vancouver, BC, Canada*, 2024.
- [25] C. Zhu, T. Wang, W. Zhang, K. Chen, and X. Liu, "Scanreason: Empowering 3d visual grounding with reasoning capabilities," in *European Conference on Computer Vision*. Springer, 2024, pp. 151–168.

- [26] I. Armeni, Z.-Y. He, J. Gwak, A. R. Zamir, M. Fischer, J. Malik, and S. Savarese, “3d scene graph: A structure for unified semantics, 3d space, and camera,” 2019. [Online]. Available: <https://arxiv.org/abs/1910.02527>
- [27] U.-H. Kim, J.-M. Park, T.-j. Song, and J.-H. Kim, “3-d scene graph: A sparse and semantic representation of physical environments for intelligent agents,” *IEEE Transactions on Cybernetics*, vol. 50, no. 12, p. 4921–4933, Dec. 2020. [Online]. Available: <http://dx.doi.org/10.1109/TCYB.2019.2931042>
- [28] J. Wald, H. Dhano, N. Navab, and F. Tombari, “Learning 3d semantic scene graphs from 3d indoor reconstructions,” in *Conference on Computer Vision and Pattern Recognition*, 2020.
- [29] A. Rosinol, A. Violette, M. Abate, N. Hughes, Y. Chang, J. Shi, A. Gupta, and L. Carlone, “Kimera: from slam to spatial perception with 3d dynamic scene graphs,” 2021. [Online]. Available: <https://arxiv.org/abs/2101.06894>
- [30] N. Hughes, Y. Chang, and L. Carlone, “Hydra: A real-time spatial perception system for 3d scene graph construction and optimization,” 2022. [Online]. Available: <https://arxiv.org/abs/2201.13360>
- [31] Z. Wang, B. Cheng, L. Zhao, D. Xu, Y. Tang, and L. Sheng, “VI-sat: Visual-linguistic semantics assisted training for 3d semantic scene graph prediction in point cloud,” *arXiv preprint arXiv:2303.14408*, 2023.
- [32] S. Koch, N. Vaskevicius, M. Colosi, P. Hermosilla, and T. Ropinski, “Open3dsg: Open-vocabulary 3d scene graphs from point clouds with queryable objects and open-set relationships,” in *Proc. Computer Vision and Pattern Recognition*, 2024, pp. 14 183–14 193.
- [33] H. Liu, C. Li, Q. Wu, and Y. J. Lee, “Visual instruction tuning,” *Advances in neural information processing systems*, vol. 36, 2024.
- [34] T. Ren, S. Liu, A. Zeng, J. Lin, K. Li, H. Cao, J. Chen, X. Huang, Y. Chen, F. Yan *et al.*, “Grounded sam: Assembling open-world models for diverse visual tasks,” *arXiv preprint arXiv:2401.14159*, 2024.
- [35] G. Mei, L. Riz, Y. Wang, and F. Poiesi, “Vocabulary-free 3d instance segmentation with vision and language assistant,” *arXiv preprint arXiv:2408.10652*, 2024.
- [36] P. Achlioptas, A. Abdelreheem, F. Xia, M. Elhoseiny, and L. Guibas, “Referit3d: Neural listeners for fine-grained 3d object identification in real-world scenes,” in *Computer Vision—ECCV 2020: 16th European Conference, Glasgow, UK, August 23–28, 2020, Proceedings, Part I 16*. Springer, 2020, pp. 422–440.
- [37] D. Z. Chen, A. X. Chang, and M. Nießner, “Scanrefer: 3d object localization in rgb-d scans using natural language,” in *European conference on computer vision*. Springer, 2020, pp. 202–221.
- [38] J. Straub, T. Whelan, L. Ma, Y. Chen, E. Wijmans, S. Green, J. J. Engel, R. Mur-Artal, C. Ren, S. Verma, A. Clarkson, M. Yan, B. Budge, Y. Yan, X. Pan, J. Yon, Y. Zou, K. Leon, N. Carter, J. Briales, T. Gillingham, E. Mueggler, L. Pesqueira, M. Savva, D. Batra, H. M. Strasdat, R. D. Nardi, M. Goesele, S. Lovegrove, and R. Newcombe, “The Replica dataset: A digital replica of indoor spaces,” *arXiv preprint arXiv:1906.05797*, 2019.
- [39] A. Dai, A. X. Chang, M. Savva, M. Halber, T. Funkhouser, and M. Nießner, “ScanNet: Richly-annotated 3d reconstructions of indoor scenes,” in *Proc. Computer Vision and Pattern Recognition, IEEE*, 2017.
- [40] L. Zhao, D. Cai, L. Sheng, and D. Xu, “3dvg-transformer: Relation modeling for visual grounding on point clouds,” in *Proc. of the IEEE/CVF International Conference on Computer Vision*, 2021, pp. 2928–2937.
- [41] A. Jain, N. Gkanatsios, I. Mediratta, and K. Fragkiadaki, “Bottom up top down detection transformers for language grounding in images and point clouds,” in *European Conference on Computer Vision*. Springer, 2022, pp. 417–433.
- [42] Y. Wang, Y. Li, and S. Wang, “G⁺ 3-lq: Marrying hyperbolic alignment with explicit semantic-geometric modeling for 3d visual grounding,” in *Proc. Computer Vision and Pattern Recognition*, 2024, pp. 13 917–13 926.
- [43] Z. Qian, Y. Ma, Z. Lin, J. Ji, X. Zheng, X. Sun, and R. Ji, “Multi-branch collaborative learning network for 3d visual grounding,” in *European Conference on Computer Vision*. Springer, 2024, pp. 381–398.
- [44] O. Unal, C. Sakaridis, S. Saha, and L. Van Gool, “Four ways to improve verbo-visual fusion for dense 3d visual grounding,” in *European Conference on Computer Vision*. Springer, 2024, pp. 196–213.
- [45] Y. Zhang, H. Luo, and Y. Lei, “Towards clip-driven language-free 3d visual grounding via 2d-3d relational enhancement and consistency,” in *Proc. Computer Vision and Pattern Recognition*, 2024, pp. 13 063–13 072.
- [46] W. Guo, X. Xu, Z. Wang, J. Feng, J. Zhou, and J. Lu, “Text-guided sparse voxel pruning for efficient 3d visual grounding,” in *Proc. Computer Vision and Pattern Recognition*, 2025, pp. 3666–3675.
- [47] Z. Wang, H. Huang, Y. Zhao, L. Li, X. Cheng, Y. Zhu, A. Yin, and Z. Zhao, “Distilling coarse-to-fine semantic matching knowledge for weakly supervised 3d visual grounding,” in *Proc. of the IEEE/CVF International Conference on Computer Vision*, 2023, pp. 2662–2671.
- [48] J. Kerr, C. M. Kim, K. Goldberg, A. Kanazawa, and M. Tancik, “Lerf: Language embedded radiance fields,” in *Proc. of the IEEE/CVF International Conference on Computer Vision*, 2023, pp. 19 729–19 739.
- [49] Z. Yuan, J. Ren, C.-M. Feng, H. Zhao, S. Cui, and Z. Li, “Visual programming for zero-shot open-vocabulary 3d visual grounding,” in *Proc. Computer Vision and Pattern Recognition*, 2024, pp. 20 623–20 633.
- [50] M. Feng, Z. Li, Q. Li, L. Zhang, X. Zhang, G. Zhu, H. Zhang, Y. Wang, and A. Mian, “Free-form description guided 3d visual graph network for object grounding in point cloud,” in *Proc. of the IEEE/CVF International Conference on Computer Vision*, 2021, pp. 3722–3731.
- [51] E. Bakr, Y. Alsaedy, and M. Elhoseiny, “Look around and refer: 2d synthetic semantics knowledge distillation for 3d visual grounding,” *Advances in neural information processing systems*, vol. 35, pp. 37 146–37 158, 2022.
- [52] Z. Yang, S. Zhang, L. Wang, and J. Luo, “Sat: 2d semantics assisted training for 3d visual grounding,” in *Proc. of the IEEE/CVF International Conference on Computer Vision*, 2021, pp. 1856–1866.
- [53] J. Luo, J. Fu, X. Kong, C. Gao, H. Ren, H. Shen, H. Xia, and S. Liu, “3d-sps: Single-stage 3d visual grounding via referred point progressive selection,” in *Proc. Computer Vision and Pattern Recognition*, 2022, pp. 16 454–16 463.
- [54] S. Huang, Y. Chen, J. Jia, and L. Wang, “Multi-view transformer for 3d visual grounding,” in *Proc. Computer Vision and Pattern Recognition*, 2022, pp. 15 524–15 533.
- [55] S. Y. Gadre, M. Wortsman, G. Ilharco, L. Schmidt, and S. Song, “Cows on pasture: Baselines and benchmarks for language-driven zero-shot object navigation,” in *Proc. Computer Vision and Pattern Recognition*, 2023, pp. 23 171–23 181.
- [56] N. Zantout, H. Zhang, P. Kachana, J. Qiu, J. Zhang, and W. Wang, “Sort3d: Spatial object-centric reasoning toolbox for zero-shot 3d grounding using large language models,” *arXiv preprint arXiv:2504.18684*, 2025.
- [57] Q. Yuan, J. Zhang, K. Li, and R. Stiefelhausen, “Solving zero-shot 3d visual grounding as constraint satisfaction problems,” *arXiv preprint arXiv:2411.14594*, 2024.
- [58] C. Zhang, J. Yu, Y. Song, and W. Cai, “Exploiting edge-oriented reasoning for 3d point-based scene graph analysis,” 2021. [Online]. Available: <https://arxiv.org/abs/2103.05558>
- [59] A. Radford, J. W. Kim, C. Hallacy, A. Ramesh, G. Goh, S. Agarwal, G. Sastry, A. Askell, P. Mishkin, J. Clark *et al.*, “Learning transferable visual models from natural language supervision,” in *International conference on machine learning*. PMLR, 2021, pp. 8748–8763.
- [60] S.-C. Wu, J. Wald, K. Tateno, N. Navab, and F. Tombari, “Scenegrphfusion: Incremental 3d scene graph prediction from rgb-d sequences,” 2021. [Online]. Available: <https://arxiv.org/abs/2103.14898>
- [61] B. Li, K. Q. Weinberger, S. Belongie, V. Koltun, and R. Ranftl, “Language-driven semantic segmentation,” *arXiv preprint arXiv:2201.03546*, 2022.
- [62] G. Ghiasi, X. Gu, Y. Cui, and T.-Y. Lin, “Scaling open-vocabulary image segmentation with image-level labels,” 2022. [Online]. Available: <https://arxiv.org/abs/2112.12143>
- [63] K. Yamazaki, T. Hanyu, K. Vo, T. Pham, M. Tran, G. Doretto, A. Nguyen, and N. Le, “Open-fusion: Real-time open-vocabulary 3d mapping and queryable scene representation,” in *2024 IEEE International Conference on Robotics and Automation (ICRA)*. IEEE, 2024, pp. 9411–9417.
- [64] Y. Wang, B. Jia, Z. Zhu, and S. Huang, “Masked point-entity contrast for open-vocabulary 3d scene understanding,” in *Proc. Computer Vision and Pattern Recognition*, 2025, pp. 14 125–14 136.
- [65] B. Cheng, A. G. Schwing, and A. Kirillov, “Per-pixel classification is not all you need for semantic segmentation,” 2021.
- [66] K. M. Jatavallabhula, A. Kuwajerwala, Q. Gu, M. Omama, T. Chen, A. Maalouf, S. Li, G. Iyer, S. Saryazdi, N. Keetha *et al.*, “Conceptfusion: Open-set multimodal 3d mapping,” *arXiv preprint arXiv:2302.07241*, 2023.
- [67] A. Takmaz, E. Fedele, R. W. Sumner, M. Pollefeys, F. Tombari, and F. Engelmann, “Openmask3d: Open-vocabulary 3d instance segmentation,” *arXiv preprint arXiv:2306.13631*, 2023.
- [68] A. Werby, C. Huang, M. Büchner, A. Valada, and W. Burgard, “Hierarchical open-vocabulary 3d scene graphs for language-grounded robot navigation,” in *First Workshop on Vision-Language Models for Navigation and Manipulation at ICRA 2024*, 2024.